BATTERY POWER EFFICIENCY OF PPM AND FSK IN WIRELESS SENSOR NETWORKS

Qiuling Tang[1], Liuqing Yang[2], Georgios B. Giannakis[3] and Tuanfa Qin[4]

[1,4] Lab of Modern Acoustics, Univ. of Nanjing, P.O.Box 2002, Nanjing, Jiangsu 210093; Dept. of CEE, Univ. of Guangxi, Nanning, Guangxi 530004, P. R. China
[2]Dept. of ECE, Univ. of Florida, P.O.Box 116130, Gainesville, FL 32611, USA
[3]Dept. of ECE, Univ. of Minnesota, 200 Union St. SE, Minneapolis, MN 55455, USA

ABSTRACT

In wireless sensor networks (WNSs), sensor nodes are usually battery-powered. Hence, energy efficiency is a critical factor in WSNs. Orthogonal modulations suitable for energy-limited WSNs have been investigated under the assumption that batteries are linear and ideal. However, these analyses are not valid when more realistic nonlinear battery models are considered. Based on a general model integrating WSN transmission modules with realistic battery models, we derive two battery power-conserving schemes for M-ary pulse position modulation (PPM) and frequency shift keying (FSK). We analyze and compare their battery power efficiencies in various wireless channels. Our results reveal that FSK is more power-efficient than PPM in sparse WSNs, while PPM may outperform FSK in dense WSNs. We also show that in sparse WSNs, the power advantage of FSK over PPM is no more than 3dB; whereas in dense WSNs, the power advantage of PPM over FSK can be significant.

INTRODUCTION

WSNs comprise a large number of densely distributed sensor nodes and have many civil and military applications. Since sensor nodes are typically small and powered by non-renewable batteries, energy efficiency is a critical factor in WSNs.

Several energy-efficient approaches, including network protocols and cross-layer designs, have been investigated in the WSN setup. At the physical layer, modulation, coding, adaptive resource allocation and cooperative relays have also been studied to improve energy efficiency (see e.g., [3], [7], [10]). However, all are built on the premise that the batteries are ideal and linear. This implies that the actual battery power consumption equals the total power required by all energy-consuming modules. But in reality, part of the battery's capacity may be wasted. Hence, the lifetime of battery-driven sensor nodes depends on not only the power required by energy-consuming modules, but also the unique nonlinear characteristics of batteries. Realistic nonlinear battery models are available [6], [8], and have been considered in the rapidly evolving area of battery-driven system design. Compared to conventional low power designs, the latter has the potential to markedly improve the lifetime of battery-powered systems [2]. However, existing battery-driven approaches have only dealt with hardware and software optimization of a single node [5], [6]; and do not consider modulation and communication issues at the physical layer. Clearly, there is a need to integrate realistic battery models in the design and evaluation of modulation and communication schemes for WSNs.

This paper explores battery-driven issues for low power modulations. We derive a general model that integrates WSN transmission and reception modules with realistic nonlinear battery models, which distinguishes our model from existing alternatives [1], [7], [10]. Compared with cellular networks, transmit power (TP) in WSNs is much smaller and is comparable to circuit power consumption (CPC). In addition, typical data rates are low and complex signal processing is not present. Thus, our general model treats power consumption for signal processing as negligible. Using this model, we evaluate the power efficiency of orthogonal PPM and FSK and quantify their *battery power efficiencies* for sparse and dense WSNs, in path-loss and fading wireless channels. Our comparisons suggest that different sensor densities and data rates favor different modulation schemes. While ensuring low-power operation of sensor nodes, our model is also unique in that it includes non-coherent detection and energy-efficient circuit work/sleep modes.

In the following sections, we put forward a general system model for battery-driven sensors; specify the modulation, transmission and detection schemes; then analyze and compare their battery power efficiencies in various channel models; finally, numerical results and concluding remarks are presented.

GENERAL SYSTEM MODEL

The diagram of a fully-functioning node is shown in Fig 1(a), which includes a transmitter, a receiver, a power-supporting battery and a DC/DC converter to generate a desired and stable supply voltage for the transmitter or the receiver. The node works with half-duplex communication mode (alternately transmitting and receiving), which is commonly used in WSNs for power efficiency. To explore the battery power consumption at the node, let us resort to a point-to-point link in the network. This link consists of

Scientific Fund of Guangxi Edu. Dept. of China No. [2002]316; NSF Grant No. EIA-0324864. Prepared through collaborative participation in the Communications and Networks Consortium sponsored by the U. S. Army Research Laboratory under the Collaborative Technology Alliance Program, Cooperative Agreement DAAD19-01-2-0011. The U. S. Government is authorized to reproduce and distribute reprints for Government purposes notwithstanding any copyright notation thereon.

a transmitting node and a receiving node, where only the transmitter in the former and the receiver in the later are switched on. Based on the link model shown in Fig. 1(b), we will figure out the battery power consumptions in the transmitting node and receiving node respectively, then we will integrate them as the battery power consumption of the fully-functioning node.

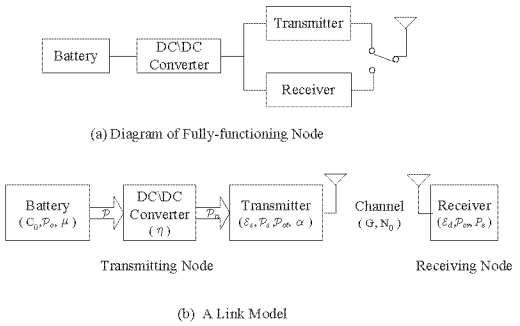

Fig. 1. System model

Let us consider the transmitting node first. To achieve a prescribed symbol error rate (SER) that satisfies quality of service (QoS) requirements, a symbol energy $\mathcal{E}_d$ is needed at the receiver. The corresponding symbol energy at the transmitter $\mathcal{E}_s$ is $\mathcal{E}_s = \mathcal{E}_d/G$, where G is the channel gain which captures the channel effects. With a rectangular pulse shaper of duration T_p, the TP is $\mathcal{P}_s = \mathcal{E}_s/T_p$. In WSNs, CPC $\mathcal{P}_{ct}$ in the transmitting node may be comparable to TP $\mathcal{P}_s$ and needs to be considered too. Hence, the total power consumption at the transmitter $\mathcal{P}_{nt}$ is given by

$$\mathcal{P}_{nt} = (1+\alpha)\mathcal{P}_s + \mathcal{P}_{ct}, \tag{1}$$

where $\alpha\mathcal{P}_s$ ($0 < \alpha < 1$) corresponds to the power consumed by the power amplifier. Factor $\alpha = \xi/\varsigma - 1$ depends on the drain efficiency ς of the RF power amplifier and the peak-to-average power ratio (PAPR) ξ of the transmitted signal. For constant modulus modulations, we have $\xi = 1$; and for class-B power amplifiers not limited to operate in the linear region, the drain efficiency is $\varsigma = 0.75$. For convenience, we will henceforth call $(1+\alpha)\mathcal{P}_s$ the total TP.

As the supply voltage required by the transmitter circuits can be different from the battery voltage V, a power-consuming DC/DC converter is needed. Therefore, to provide the total power $\mathcal{P}_{nt}$ at the transmitting node, the power drawn from the battery (discharge power) is $\mathcal{P}_t = \mathcal{P}_{nt}/\eta$, where $\eta < 1$ is the transfer efficiency of the DC/DC converter. If the battery is linear, then its power consumption is identical to its discharge power. However, batteries are generally nonlinear and part of their stored energy (capacity) is wasted when they release energy to drive the transmitter. The main capacity-related nonlinearity is known as rate capacity effect[5]. If the discharge current is small, the stored energy will be completely used or released. In this case, the battery can be considered as linear. But if the discharge current has large magnitude, nonlinearities emerge and considerable portion of the stored energy is wasted. The amount of wasted energy heavily depends on the discharge current profile. In this paper, we will consider the rate capacity effect in our model.

Let C_0 denote the capacity of a new battery, defined as the total energy it stores. It is related to the energy C actually consumed by the source node through the so-termed battery efficiency factor: $\mu := C/C_0$. Accordingly, the actual power used in the battery is $\mathcal{P}_t/\mu = VI_t/\mu$, where V and I_t are the discharge voltage and current during a pulse interval. Corroborated with experiments, two models are available to describe the relationship between discharge current and efficiency [6]

$$\mu(I_t) = 1 - \omega I_t, \tag{2}$$

$$\text{and} \quad \mu(I_t) = 1 - \nu I_t^2, \tag{3}$$

where ω and ν are both positive constants. The battery efficiency factor μ varies from $\mu_{\max}$ to $\mu_{\min}$ when the discharge current increases from the rated minimum $I_{\min}$ to the rated maximum $I_{\max}$. Generally, $\mu_{\max} = 1$ and $\mu_{\min}$ can be as small as 0.5 [6].

Let us consider the discharge current waveforms in a low-data-rate sensor communication system, which are similar to the transmit current profiles shown in Fig. 2. If i_t denotes the instantaneous discharge current with probability density function (pdf) $f(i_t)$, the actual power consumption of the battery is $Vi_t/\mu(i_t)$. It follows that the average actual power consumption (AAPC) of the battery can be expressed as

$$\mathcal{P}_{0t} = V \int_{I_{\min}}^{I_{\max}} \frac{i_t}{\mu(i_t)} f(i_t)\, di_t. \tag{4}$$

The important implication of the last expression is that even with the same battery parameters (ω or ν), different modulation schemes and circuit operation modes will give rise to different $f(i_t)$'s and thus different battery AAPCs. For a fixed current mean value $E\{i_t\}$, the minimum battery AAPC $\mathcal{P}_{0t}$ occurs when i_t follows a single δ-function distribution and $\mathcal{P}_{0t}$ is maximized when i_t is uniformly distributed [6].

As for the receiving node, assuming it is powered by a battery through a DC/DC converter with the same parameters as those for the transmitting node, the above battery power consumption model for transmitting node can be used for the receiving node by replacing the total power consumption expression (1) for the transmitter with $\mathcal{P}_{nr} = \mathcal{P}_{cr}$ for the receiver because there is no TP and only the CPC needs to be considered at the receiving node. It is worth mentioning that the variables about power and discharge current of the receiving node are distinguished by a subscript 'r' from those for the transmitting node with a subscript 't'.

Having obtained the AAPCs for the transmitting node and the receiving node, the battery AAPC for the fully-functioning node is

$$\mathcal{P}_0 = \frac{1}{2}\mathcal{P}_{0t} + \frac{1}{2}\mathcal{P}_{0r} \tag{5}$$

since it works with half-duplex communication mode.

With battery capacity C_0 and AAPC $\mathcal{P}_0$, the battery lifetime is $C_0/\mathcal{P}_0$. Obviously, smaller $\mathcal{P}_0$ implies longer battery lifetime. Therefore, battery AAPC $\mathcal{P}_0$ measures battery power efficiency.

So far, we have established a general battery-driven system model. Based on this model, we will evaluate the battery power efficiency of two orthogonal modulations.

PERFORMANCE OF PPM AND FSK

In this section, we rely on power-efficient orthogonal modulations to derive battery power-conserving schemes tailored for WSNs. Our schemes use non-coherent detection and take into account power-efficient circuit work/sleep operating modes, carrier transmissions, low power low-IF transceiver design, and the nonlinear battery models we outlined in the previous section.

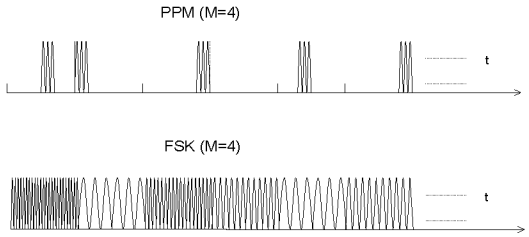

Fig. 2. Transmit current waveforms for PPM and FSK with $M = 4$

FSK and PPM are both common orthogonal modulation. FSK signal is known to be transmitted by carrier while PPM can afford carrier and baseband transmission. In our low data rate setup for WSNs, we consider carrier transmission for both FSK and PPM. Both M-ary FSK and PPM with rectangular transmitted current waveforms, as in Fig. 2, have the same bandwidth efficiency $B_e = k/M$, where $k = \log_2 M$ is the number of bits per symbol. As the constellation size M increases, bandwidth efficiency B_e decreases, but the required energy for transmitting a bit also decreases for any preset error probability. The price paid for this power efficiency is longer symbol duration in PPM and larger bandwidth in FSK. Being orthogonal, they both enable constant-modulus transmissions during their pulse intervals and can afford low-complexity non-coherent detection. Here, we establish SER upper bounds for M-ary orthogonal modulations with non-coherent detection over various channels (see [9] for the proof):

Lemma 1: *If G denotes the channel gain and N_0 the spectral density of the AWGN, the instantaneous SER for M-ary orthogonal signaling in AWGN with non-coherent detection is upper-bounded by*

$$P_e \leq 1 - \left(1 - 0.5e^{-\frac{1}{2}G\frac{\mathcal{E}_s}{N_0}}\right)^{M-1} .$$

This bound is universally tighter than the union bound $\forall \mathcal{E}_s/N_0$ and $\forall M$ but $M = 2$.

Based on Lemma 1, the transmit energy per symbol for any prescribed SER P_e in AWGN and path-loss channels is approximately:

$$\mathcal{E}_s = 2N_0 G^{-1} \ln\left(2\left(1 - (1 - P_e)^{\frac{1}{M-1}}\right)\right)^{-1} . \quad (6)$$

In fading channels, however, the average SER needs to be considered:

Lemma 2: *In Rayleigh fading channels, $\bar{G} := \mathrm{E}\{G\}$, the average SER for M-ary orthogonal signaling with non-coherent detection is upper bounded by*

$$\bar{P}_e \leq 1 - \left(1 - \frac{1}{2 + \bar{G}\frac{\mathcal{E}_s}{N_0}}\right)^{M-1} , \quad \forall M, \quad \mathcal{E}_s/N_0 .$$

Using Lemma 2, the transmit energy per symbol for any prescribed average SER in Rayleigh fading channels is approximately

$$\mathcal{E}_s = N_0 \bar{G}^{-1} \left(\left(1 - (1 - \bar{P}_e)^{\frac{1}{M-1}}\right)^{-1} - 2\right). \quad (7)$$

Eqs. (6) and (7) can be readily applied to PPM and FSK for path-loss and Rayleigh fading channels respectively.

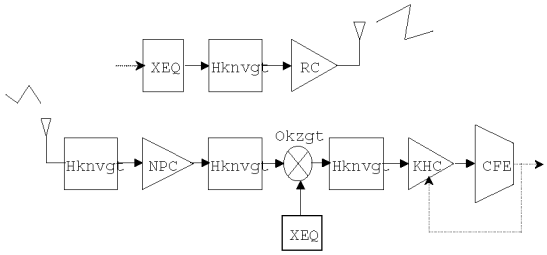

Fig. 3. Transceiver analog circuit blocks

Based on a generic low-intermediate frequency (low-IF) transceiver structure, both FSK and PPM with carrier transmission can share a similar analog circuit model shown in Fig. 3. At the transmitter, for FSK, signal is modulated by switching on different control voltages for a voltage control oscillator (VCO) to generate the required radio frequencies. For PPM, a VCO is also needed to carry out the carrier modulation. After modulation, RF signal waveform is amplified and transmitted out from an antenna. At the receiver, the received RF signal is first converted to an IF signal, then demodulated and envelop-detected in the baseband digitally. Specifically, the received RF signal is first filtered by a frontend filter and amplified by a low noise amplifier (LAN); after cleaned by an anti-aliasing filter, it is down-converted by a mixer; then filtered again, it goes through the IF amplifier (IFA) whose gain is adjustable; finally it is converted to a digital signal via the analog-to-digital converter (ADC) and then have demodulation and processing digitally. Based on this circuit model, the power consumption at the transmitter $\mathcal{P}_{ct}$ is

$$\mathcal{P}_{ct} = \mathcal{P}_{LO} + \mathcal{P}_{filt} \quad (8)$$

and at the receiver $\mathcal{P}_{cr}$ is

$$\mathcal{P}_{cr} = \mathcal{P}_{LO} + \mathcal{P}_{mix} + \mathcal{P}_{LNA} + \mathcal{P}_{filr} + \mathcal{P}_{IFA} + \mathcal{P}_{ADC}, \quad (9)$$

where $\mathcal{P}_{LO}$ is the power consumption of VCO and $\mathcal{P}_{filt}$ is that of the filter at the transmitter. $\mathcal{P}_{mix}$, $\mathcal{P}_{LNA}$, $\mathcal{P}_{filr}$, $\mathcal{P}_{IFA}$ and $\mathcal{P}_{ADC}$ denote the powers consumed in the mixer, LAN, filter, IFA and ADC at the receiver, respectively.

So far, we have seen that PPM and FSK share the same bandwidth efficiency and SER performance, and a similar RF transceiver structure. However, Fig. 2 testifies that their transmitted signals are quite different. This difference implies distinct circuit operating modes, discharge current pdfs and thereby battery AAPC's. These differences can be summarized as follows:

1. To achieve a given SER P_e (or $\bar{P}_e$), PPM and FSK require identical transmit energy per symbol. Hence, the TPs for PPM ($\mathcal{P}_s^p$) and FSK ($\mathcal{P}_s^f$) are related via: $\mathcal{P}_s^p(M) = M\mathcal{P}_s^f(M)$, simply because $T_p = T_s/M$ with PPM, and $T_p = T_s$ with FSK. Mention again, in this paper, the superscript 'p' and 'f' are used to distinguish the variables for PPM and FSK respectively.
2. As to CPC, differences arise in their circuit operating modes. Because PPM has active and idle intervals, by turning on and off the circuits according to the transmission state, we consider here a sleep mode during idle intervals at both transmitter and receiver. On the other hand, FSK is always in an active mode. This difference will turn out to have major impact in the battery power efficiency comparisons that we will pursue in the next section.
3. Their discharge current pdfs are different:

$$\begin{array}{l} f(i^p) = \frac{1}{M}\delta(i^p - I^p) + \frac{M-1}{M}\delta(i^p) \quad \text{and} \\ f(i^f) = \delta(i^f - I^f), \end{array} \tag{10}$$

   where i^p and i^f are the discharge currents for PPM and FSK, and I^p and I^f are their corresponding values in active mode. The pdfs can be used in both the transmitting node and the receiving node by adding their corresponding subscript 't' and 'r' to the current variables in (10).
4. In addition to their distinct operating modes, the CPCs for FSK and PPM are also different because their components and devices are not identical. The difference at the transmitter is captured by a factor θ_t with $\mathcal{P}_{ct}^p = \theta_t\mathcal{P}_{ct}^f$ and commonly $\theta_t < 1$. Similarly, a factor θ_r can be used at the receiver with $\mathcal{P}_{cr}^p = \theta_t\mathcal{P}_{cr}^f$, and $\theta_r < 1$.

Summarily, both FSK and PPM are power-efficient modulations. Both can afford low-complexity non-coherent detection and have a similar RF transceiver structure. While PPM enables sleep mode during idle intervals, FSK enjoys the optimal discharge current distribution: a single δ function, which minimizes the battery AAPC if the mean of the discharge current remains invariant.

To facilitate battery power efficiency comparison between the two modulation schemes, we define the ratio of their corresponding AAPCs as battery power efficiency ratio (BPER)

$$R_e := 10\log\left(\mathcal{P}_0^p/\mathcal{P}_0^f\right). \tag{11}$$

In the ensuing sections, we will quantify R_e for different wireless propagation channels.

BATTERY POWER EFFICIENCY COMPARISONS

Substituting the results in previous Section into our general system model, at the transmitting node, the TPs of PPM and FSK can be expressed in terms of their transmit energy per symbol as [cf. (6) and (7)]:

$$\mathcal{P}_s^p = \frac{\mathcal{E}_s}{T_p} = \mathcal{E}_s B \quad \text{and} \quad \mathcal{P}_s^f = \frac{\mathcal{E}_s}{T_s} = \frac{\mathcal{E}_s B}{M}\ .$$

Setting the CPC for FSK $\mathcal{P}_{ct}^f = \mathcal{P}_{ct}$, it follows that the total power consumption for PPM and FSK at the transmitter module is

$$\mathcal{P}_{nt}^p = \mathcal{E}_s\beta + \theta_t\mathcal{P}_{ct} \quad \text{and} \quad \mathcal{P}_{nt}^f = \frac{\mathcal{E}_s\beta}{M} + \mathcal{P}_{ct}\ ,$$

where $\beta := (1+\alpha)B$ for convenience. Their corresponding discharge currents in active mode can then be expressed as

$$I_t^p = \frac{1}{V\eta}\left(\mathcal{E}_s\beta + \theta_t\mathcal{P}_{ct}\right) \text{ and } I_t^f = \frac{1}{V\eta}\left(\frac{\mathcal{E}_s\beta}{M} + \mathcal{P}_{ct}\right). \tag{12}$$

Substituting (10) and (12) into (4), the battery AAPCs for PPM and FSK at the transmitting node can be obtained as

$$\begin{array}{l} \mathcal{P}_{0t}^p = \frac{1}{\eta}\cdot\frac{\mathcal{E}_s\beta+\theta\mathcal{P}_{ct}}{M}\cdot\frac{1}{\mu(I_t^p)} \quad \text{and} \\ \mathcal{P}_{0t}^f = \frac{1}{\eta}\cdot\left(\frac{\mathcal{E}_s\beta}{M} + \mathcal{P}_{ct}\right)\cdot\frac{1}{\mu(I_t^f)}\ . \end{array} \tag{13}$$

As for the receiving node, owing to no TP and letting the CPC for FSK be $\mathcal{P}_{cr}^f = \mathcal{P}_{cr}$, the total power consumption in the receiver module is that

$$\mathcal{P}_{nr}^p = \theta_r\mathcal{P}_{cr}, \quad \text{for PPM,} \quad \text{and} \quad \mathcal{P}_{nr}^f = \mathcal{P}_{cr}, \quad \text{for FSK.}$$

Similarly, with the associated discharge currents

$$I_r^p = \frac{\theta_r\mathcal{P}_{cr}}{V\eta}, \quad \text{for PPM,} \quad \text{and} \quad I_r^f = \frac{\mathcal{P}_{cr}}{V\eta}, \quad \text{for FSK,}$$

and the pdfs expressed in (10), we can derive their battery AAPCs to be that

$$\mathcal{P}_{0r}^p = \frac{1}{\eta}\cdot\frac{\theta_r\mathcal{P}_{cr}}{M}\cdot\frac{1}{\mu(I_t^p)} \quad \text{and} \tag{14}$$

$$\mathcal{P}_{0r}^f = \frac{1}{\eta}\cdot\mathcal{P}_{cr}\cdot\frac{1}{\mu(I_r^f)}\ . \tag{15}$$

Accordingly, for a full-functioning node with half-duplex communication mode, the battery AAPCs for PPM and FSK are obtained from (5) that

$$\begin{array}{l} \mathcal{P}_0^p = \frac{1}{2\eta M}\cdot\left((\mathcal{E}_s\beta + \theta_t\mathcal{P}_{ct})\cdot\frac{1}{\mu(I_t^p)} + \theta_r\mathcal{P}_{cr}\cdot\frac{1}{\mu(I_r^p)}\right) \text{ and} \\ \mathcal{P}_0^f = \frac{1}{2\eta M}\cdot\left((\mathcal{E}_s\beta + M\mathcal{P}_{ct})\cdot\frac{1}{\mu(I_t^f)} + M\mathcal{P}_{cr}\cdot\frac{1}{\mu(I_r^f)}\right). \end{array} \tag{16}$$

Then, by the definition of BPER, we have

$$R_e = 10\log\left(\frac{(\mathcal{E}_s\beta + \theta_t\mathcal{P}_{ct})\frac{1}{\mu(I_t^p)} + \theta_r\mathcal{P}_{cr}\cdot\frac{1}{\mu(I_r^p)}}{(\mathcal{E}_s\beta + M\mathcal{P}_{ct})\frac{1}{\mu(I_t^f)} + M\mathcal{P}_{cr}\cdot\frac{1}{\mu(I_r^f)}}\right). \tag{17}$$

Evidently, FSK is more battery power-efficient if $R_e > 0$, and vice versa. In the ensuing subsections, we will evaluate R_e for path-loss and Rayleigh fading channels. As the density of WSNs determines the average inter-sensor

distance and thus the TP, we will consider two scenarios for each channel model: sparsely-deployed sensors and densely-deployed sensors. In the former scenario, the CPC is much smaller than the TP and is thus negligible; whereas in the latter scenario, the CPC is comparable to the TP and cannot be neglected.

A. PATH-LOSS CHANNEL

For a K^{th}-power path-loss channel, the channel gain G_d depends on the transceiver distance d and is given by $G_d = \mathcal{P}_s/\mathcal{P}_d = M_l d^K G_1$, where the link margin M_l accounts for the effects of transceiver hardware, residual additive background interference, and G_1 is the gain factor at $d = 1$ which is specified by the antenna gain, carrier frequency and other system parameters. With $G = 1/G_d$, the transmit energy per symbol in Eq. (6) is a function of both M and d:

$$\mathcal{E}_s(M,d) = 2N_0 M_l G_1 d^K \ln\left(2 - 2(1-P_e)^{\frac{1}{M-1}}\right)^{-1}. \quad (18)$$

Hence, the corresponding discharge currents, battery AAPC and BPER all are functions of M and d. Additionally, we prove in [9] the following properties of $\mathcal{E}_s(M,d)$:

Lemma 3: *The required energy per symbol in path-loss channels $\mathcal{E}_s(M,d)$ is a monotonically increasing function of M, $\forall P_e$; while $\mathcal{E}_s(M,d)/M$ is a monotonically decreasing function of M for the practical SER range $P_e \leq 0.0677$.*

With Lemma 3, we are now ready to compare the battery power efficiency of PPM and FSK for sparse and dense WSNs. For a clear development, we start with the sparse case.

A.1. Sparse WSNs: When the CPC is considered to be negligible compared with the TP, i.e., when $\mathcal{P}_{ct} = 0$ and $\mathcal{P}_{cr} = 0$, the battery AAPCs in (16) turns out to be

$$\begin{aligned}\mathcal{P}_0^p(M,d) &= \tfrac{1}{2\eta}\tfrac{\mathcal{E}_s(M,d)\beta}{M}\tfrac{1}{\mu(I_t^p(M,d))} \quad \text{and} \\ \mathcal{P}_0^f(M,d) &= \tfrac{1}{2\eta}\tfrac{\mathcal{E}_s(M,d)\beta}{M}\tfrac{1}{\mu(I_t^f(M,d))},\end{aligned} \quad (19)$$

where the discharge current $I_t^p(M,d)$ and $I_t^f(M,d)$ can be obtained from (12) as

$$I_t^p(M,d) = \frac{\mathcal{E}_s(M,d)\beta}{V\eta} \text{ and } I_t^f(M,d) = \frac{\mathcal{E}_s(M,d)\beta}{MV\eta}. \quad (20)$$

equation Then, the resulting BPER is that

$$R_e(M,d) = 10\log\left(\frac{\mu(I_t^f(M,d))}{\mu(I_t^p(M,d))}\right). \quad (21)$$

Evaluating $R_e(M,d)$, we obtain the following result.

Proposition 1: *In sparse WSNs over pass-loss channels, where the CPC is neglected, the following results hold true:*

i) *FSK is more battery power-efficient than PPM $\forall M$ and $\forall d$.*
ii) *For a fixed d, the power advantage of FSK over PPM increases as M increases.*
iii) *For a fixed M, the power advantage of FSK over PPM increases as d increases.*
iv) *The advantage of FSK over PPM is at most 3dB; that is, $\max\{R_e(M,d)\} < 3dB$, $\forall M, d$.*

Proof: see [9].

It appears from Proposition 1 that one should always prefer FSK $\forall M, d$. But if the CPC is taken into account, we will arrive at a different conclusion.

A.2. Dense WSNs:

When CPC $\mathcal{P}_{ct} \neq 0$ and $\mathcal{P}_{cr} \neq 0$, the according battery discharge currents, battery AAPCs and BPER have all already presented at the beginning of this section from (12) to (16). In fact, when a node operates as a receiver and there is only CPC, the battery generally discharges linearly, that is:

$$\mu(I_r^p(M,d)) \approx \mu_{\max}, \quad \text{and} \quad \mu(I_r^f(M,d)) \approx \mu_{\max}. \quad (22)$$

Hence, we can rewrite (17) as

$$R_e(M,d) = 10\log\left(\frac{(\mathcal{E}_s(M,d)\beta+\theta_t\mathcal{P}_{ct})\cdot\frac{1}{\mu(I_t^p(M,d))}+\theta_r\mathcal{P}_{cr}\cdot\frac{1}{\mu_{\max}}}{(\mathcal{E}_s(M,d)\beta+M\mathcal{P}_{ct})\cdot\frac{1}{\mu(I_t^f(M,d))}+M\mathcal{P}_{cr}\cdot\frac{1}{\mu_{\max}}}\right). \quad (23)$$

When $\mathcal{P}_{ct} = 0$ and $\mathcal{P}_{cr} = 0$, $R_e(M,d)$ simplifies to (21) and is positive. But at the transmitter, as $\mathcal{P}_{ct}$ increases, the discharge currents I_t^p and I_t^f in (12) increase by the same order of magnitude and so do the battery AAPCs $\mathcal{P}_{0t}^p$ and $\mathcal{P}_{0t}^f$ in (13). Pdfs of the discharge currents i_t^p and i_t^f in (10) indicate that the mean $\bar{i_t}^f$ increases more rapidly than $\bar{i_t}^p$. Consequently, $\mathcal{P}_{0t}^f$ increases more rapidly than $\mathcal{P}_{0t}^p$. Also at the receiver, Eqs. (14) and (22) show that $\mathcal{P}_{0r}^f \geq \mathcal{P}_{0r}^p, \forall M$ and their difference rises when $\mathcal{P}_{cr}$ increases. It is expected that, when circuit power $\mathcal{P}_{ct}$ and $\mathcal{P}_{cr}$ exceeds certain values, $\mathcal{P}_0^f$ will be greater than $\mathcal{P}_0^p$ and the BPER $R_e(M,d)$ becomes negative, rendering PPM more battery power-efficient than FSK. Since the $\mathcal{P}_{ct}$ and $\mathcal{P}_{cr}$ threshold for which $R_e(M,d) = 0$ is not analytically tractable, we will resort to a lower bound $\mathcal{P}_{cl}(M,d)$. From (23), we have

$$\begin{aligned}R_e(M,d) &< 10\log\left(\frac{\mathcal{E}_s(M,d)\beta+\theta_t\mathcal{P}_{ct})\frac{1}{\mu_{\min}}+\theta_r\mathcal{P}_{cr}\frac{1}{\mu_{\max}}}{\mathcal{E}_s(M,d)\beta+M\mathcal{P}_{ct})\frac{1}{\mu_{\max}}+M\mathcal{P}_{cr}\frac{1}{\mu_{\max}}}\right) \\ &= 10\log\left(\frac{\mathcal{E}_s(M,d)\beta+\theta\mathcal{P}_c}{\mathcal{E}_s(M,d)\beta+M\mathcal{P}_c}\cdot\frac{\mu_{\max}}{\mu_{\min}}\right).\end{aligned}$$

where $\mathcal{P}_c = \mathcal{P}_{ct} + \mathcal{P}_{cr}$, $\theta = \theta_t - (\theta_t - \theta_r\frac{\mu_{\min}}{\mu_{\max}})\frac{\mathcal{P}_{cr}}{\mathcal{P}_c}$ and $0 < \theta < 1$ with the assumption of $\frac{\mu_{\min}}{\mu_{\max}} < \theta_t \leq 1$. Notice that so long as $10\log\left(\frac{\mathcal{E}_s(M,d)\beta+\theta\mathcal{P}_c}{\mathcal{E}_s(M,d)\beta+M\mathcal{P}_c}\cdot\frac{\mu_{\max}}{\mu_{\min}}\right) < 0$, it is guaranteed that $R_e(M,d) < 0$. Hence,

$$\begin{aligned}\mathcal{P}_c > \mathcal{P}_{cl}(M,d) &:= \tfrac{\beta(\mu_{\max}-\mu_{\min})}{\mu_{\min}M-\theta\mu_{\max}}\cdot 2N_0M_lG_1d^K \\ &\cdot\ln\left(2\left(1-(1-P_e)^{\frac{1}{M-1}}\right)\right)^{-1}, \quad \forall M,d,\end{aligned} \quad (24)$$

where in establishing (24), we used the fact that $\mu_{\min}M \geq 2\mu_{\min} > 1 > \theta\mu_{\max}$. When $\mathcal{P}_c \geq \mathcal{P}_{cl}(M,d)$, we have $R_e(M,d) < 0$ and PPM outperforms FSK. Furthermore, this critical power $\mathcal{P}_{cl}(M,d)$ has the following property (see [9] for proof):

Lemma 4: *The critical power $\mathcal{P}_{cl}(M,d)$ is a monotonically decreasing function of M for the practical range $P_e \leq$*

0.0677; *it is also a monotonically increasing function of* d, $\forall P_e < 0.5$.

Based on Lemma 4 and (23), we next compare the battery power efficiency of PPM and FSK:

Proposition 2: *In dense WSNs over* K*th power path-loss channels without fading, CPC* $\mathcal{P}_c$ *is non-negligible and the following results hold true:*

i) *For any* (M, d) *pair, there exists a critical power* $\mathcal{P}_{cl}(M, d)$ *as in* (24) *such that when* $\mathcal{P}_c > \mathcal{P}_{cl}(M, d)$, $R_e(M, d) < 0$ *and PPM is more battery power-efficient than FSK.*

ii) *For any given* d, *if* $\mathcal{P}_c > \mathcal{P}_{cl}(2, d)$, *then PPM has a power advantage over FSK* $\forall M$.

iii) *For any given* d, *if* $\mathcal{P}_c \leq \mathcal{P}_{cl}(2, d)$, *there exists a critical constellation size* $M_0 \geq 2$, *beyond which PPM has power advantage over FSK* $\forall M \geq M_0$.

iv) *For any given* M, *there exists a critical distance* d_0, *within which PPM has power advantage over FSK* $\forall d \leq d_0$.

v) *For small* d *that makes* $\mathcal{P}_c = \mathcal{P}_{ct} + \mathcal{P}_{cr} \gg \mathcal{E}_s(M, d)\beta$, *BPER* $R_e(M, d) \approx 10\log(\theta/M)$, *and the power advantage of PPM over FSK is very significant for large* M.

Proof: See [9]

So far, we have seen that in path-loss channels, FSK is more battery power-efficient $\forall M, d$ in sparse WSNs with the advantage upper bounded by 3dB; whereas PPM can be more battery efficient in dense WSNs with a more significant power advantage. Next, we will consider Rayleigh fading channels with path-loss effects.

B.RAYLEIGH FADING EFFECTS

In Rayleigh fading channels, the transmit energy per symbol for a preset average SER $\bar{P}_e$ is given by (7). When both fading and path-loss effects are considered, the instantaneous channel gain becomes $G = \phi^2/G_d$, where $G_d = M_l d^K G_1$ models the path-loss effect and ϕ is the Rayleigh distributed attenuation factor. Consequently, ϕ^2 is χ^2 distributed with two degrees of freedom and $\mathrm{E}\{\phi^2\} = 1$. Hence, the transmit energy per symbol in (7) can be rewritten as

$$\mathcal{E}_s'(M, d) = N_0 M_l G_1 d^K \left(\left(1 - (1 - \bar{P}_e)^{\frac{1}{M-1}} \right)^{-1} - 2 \right),$$

where the prime $'$ is used to differentiate this subsection's quantities in the presence of fading. As expected, the transmit energy per symbol is again a function of M and d.

B.1. Sparse WSNs: With $\mathcal{P}_c = 0$, the discharge currents for PPM and FSK, as well as their corresponding battery AAPCs have the same form as in (20) and (19), with $\mathcal{E}_s(M, d)$ replaced by $\mathcal{E}_s'(M, d)$. Not surprisingly, we have $R_e'(M, d) = 10\log(\mu(I_t^{f\prime}(M, d))/\mu(I_t^{p\prime}(M, d))) > 0$, and the following results:

Proposition 3: *In sparse WSNs over Rayleigh fading channels with path-loss effects, and when CPC is ignored, results i), iii) and iv) in Proposition 1 hold true. Additionally, with the same (average) SER requirement, we have* $R_e'(M, d) > R_e(M, d)$, $\forall M, d$; *that is, channel fading induces an increase of the FSK power advantage over PPM.*

Proof: see [9].

Albeit larger, notice that the power advantage of FSK over PPM is still upper bounded by 3dB.

B.2. Dense WSNs: In this case, the discharge currents for PPM and FSK, as well as their corresponding battery AAPCs have the same form as those from (12) to (16), with $\mathcal{E}_s(M, d)$ replaced by $\mathcal{E}_s'(M, d)$. So do the corresponding BPER $R_e'(M, d)$ and the critical power $\mathcal{P}_{cl}'(M, d)$. Consequently, we have the results as follow:

Proposition 4: *In dense WSNs over Rayleigh fading channels with path-loss effects, results i), iv) and v) in Proposition 2 hold true. Additionally, with the same (average) SER requirement, we have* $R_e'(M, d) > R_e(M, d)$, $\forall M, d$.

Proof: see [9].

NUMERICAL RESULTS

To provide some intuitions on the theoretical analysis, we will present quantitative results for Propositions 1-4 by an example of the system shown in Fig. 1(a). The system parameters are listed in Table I.

First, we consider sparse WSNs. Corresponding to Propositions 1 and 3, Fig. 4 illustrates that the BPER $R_e > 0$ and FSK outperforms PPM $\forall d$ when M =2, 4, 8 in both path-loss and fading channels. And the BPER increases as d increases. It can also be expected from the figure that FSK has power advantage over PPM $\forall M$ when d is specified. Moreover, we notice that BPER ≤ 3 dB in sparse WSNs.

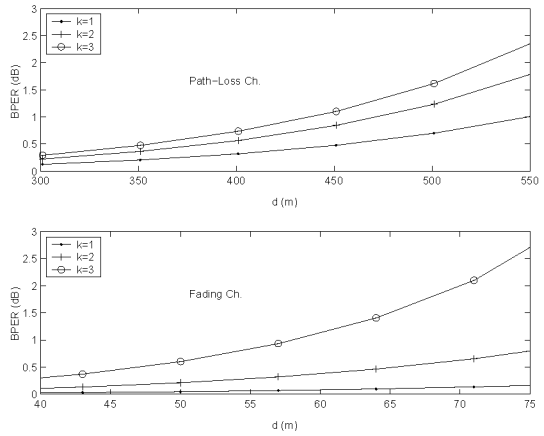

Fig. 4. BPER over transmission distance d with k=1, 2, 3 in Sparse WSNs

Then, we investigate the power advantage regions of PPM and FSK in dense WSNs. Fig. 5 provides insight about

TABLE I
SYSTEM PARAMETERS

$V = 4.2$ V	$I_{\max} = 10$A	$I_{\min} = 0$A
$\mu_{\max} = 1$	$\mu_{\min} = 0.49$	$\eta = 0.8$
$f_c = 2.5$ GHz	$\theta_t = 0.8$	$\theta_r = 0.95$
$\mathcal{P}_{syn} = 50$ mW	$\mathcal{P}_{filt} = 2.5$ mW	$\mathcal{P}_{LAN} = 20$ mW
$\mathcal{P}_{mix} = 30.3$ mW	$\mathcal{P}_{IFA} = 3$ mW	$\mathcal{P}_{filr} = 2.5$ mW
$K = 3.0$	$G_1 = 30$ dB	$M_l = 40$ dB
$\frac{N_0}{2} = -164$ dBm/Hz	$B = 10$KHz	$P_e = 10^{-3}$

the existence of critical power $\mathcal{P}_{cl}(M,d)$ and $\mathcal{P}'_{cl}(M,d)$ for all pairs (M, d) as asserted under i) in Propositions 2 and 4, and the monotonically-decreasing properties of $\mathcal{P}_{cl}(M,d)$ over M and d described in Lemma 4. It also shows the PPM and FSK advantage regions over M when $d = 150$m, and over d when $M = 4$ with critical points M_0 and d_0 for path-loss channel, and d'_0 for the fading channel;We observe that $\mathcal{P}'_{cl}(M,d) > \mathcal{P}_c \ \forall M$ in the first plot of the figure, which confirms that FSK outperforms PPM $\forall M$ when $d = 40$m in fading channel. What's more, the advantage regions of PPM and FSK can also be shown on the 2D (M, d) plane. They are distinguished by the critical curves $\mathcal{P}_{cl}(M,d) = \mathcal{P}_c$ for the path-loss channel and $\mathcal{P}'_{cl}(M,d) = \mathcal{P}_c$ for the fading channel, which are shown in the first plot of Fig. 6. The area above each critical curve is the advantage region of FSK for the corresponding channel and the areas below them are their advantage regions of PPM. We notice that in very dense WSNs, PPM outperforms FSK $\forall M$ in both channels. It is clear that PPM dominates short-term transmission (dense WSNs) as FSK does in long-term transmission (sparse WSNs).

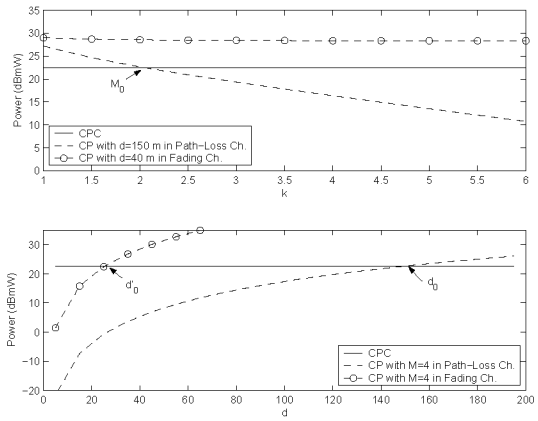

Fig. 5. CPC $\mathcal{P}_c$, critical power (CP) $\mathcal{P}_{cl}$ and advantage regions for PPM and FSK versus k (Plot 1) and d (plot 2) in Dense WSNs

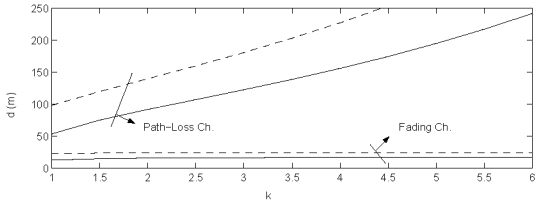

Fig. 6. Critical curves for PPM and FSK advantage regions on (M,d) plane in Dense WSNs

Finally, we give the BPER numerical values in dense WSNs for both channels. Fig. 7 shows that, in small transmission distance, $d = 30$m in path-loss channel and $d = 5$m in fading channel, their according BPERs $R_e < -15$ dB when $k = 6$ ($M = 64$) and the power advantage of PPM over FSK is very significant, as claimed by v) in Proposition 2 and 4. Also, we observe that $R'_e(M,d) > R_e(M,d)$ for all M when $d = 30$m in the figure, which corresponds to the result of Proposition 4.

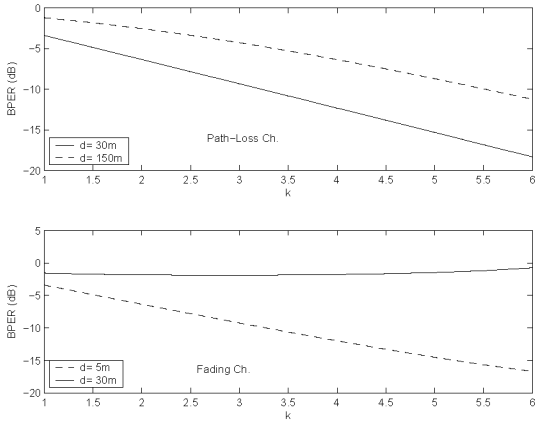

Fig. 7. BPER versus k in Dense WSNs

CONCLUSIONS

We compared the battery energy efficiency for PPM and FSK. Analysis and numerical results revealed that: i) In sparse WSNs with negligible CPC, FSK has power efficiency advantage over PPM with any constellation sizes M and transmit distances d. ii) The power efficiency advantage of FSK over PPM is no more than 3 dB. iii) As transmission distance decreases, the advantage regions of PPM and FSK changes with M and d; and iv) In dense WSNs, when CPC dominates the total power consumption of sensors, PPM outperforms FSK for all M and the power efficiency advantage is significant, especially when M is large.

References

[1] S. Cui, A. J. Goldsmith and A. Bahai, "Energy-Constranined Modulation Optimization," *IEEE Trans. on Wireless Comm.*, 2005; available at http://wsl.stanford.edu/Publications.html

[2] K. Lahiri, A. Raghunathan, S. Dey, D. Panigrahi, "Battery-Driven System Design: A New Frontier in Low Power Design," in *Proc. of the 15th Intl. Conf. on VLSI Design*, 2002, pp. 261-267.

[3] J. N. Laneman, D. N. C. Tse, and G. W. Wornell, "Cooperative Diversity in Wireless Networks: Efficient Protocols and Outage Behavior," *IEEE Trans. on Info. Theory* vol. 50, Dec. 2004, pp. 3062-3080.

[4] T. H. Lee, *The Design of CMOS Radio-Frequency Integrated Circuits*, Cambridge University Press, Cambridge, U.K., 1998.

[5] T. L. Martin, "Nonindeal Battery Properties and Their Impact on Software Design for Wearable Computers," *IEEE Trans. on Computers*, vol. 52, Aug. 2003, pp. 979-984.

[6] M. Pedram and Q. Wu, "Design Considerations for Battery-Powered Electronics," *Proc. of the 36th ACM/IEEE Conf. on Design Automation*, 1999, pp. 861-866.

[7] Y. Prakash, S. K. S. Gupta, "Energy Efficient Source Coding and Modulation for Wireless Applications," *Proc. of WCNC*, Mar. 2003, pp. 212-217.

[8] D. Rakhmatov and S. Vrudhula, "Time to Failure Estimation for Batteries in Portable systems," *Proc. of Intl. Symp. on Low Power Electr. & Design*, Aug. 2001, pp. 88-91.

[9] Q. Tang, L. Yang, G. B. Giannakis, and T. Qin, "Battery Power Efficiency of PPM and FSK in Wireless Sensor Networks," *Submitted to IEEE Trans. on Wireless Comm.*, 2004; available at http://spincom.ece.umn.edu/journalsubmit.html

[10] A. Y. Wang, C. SeongHwan, C. G. Sodini and A. P. Chandrakasan, "Energy Efficient Modulation and MAC for Asymmetric RF Microsensor Systems," *Proc. of the Intl. Symp. on Low Power Electr. & Design*, Aug. 2001, pp. 106-111.